FRONTIERS OF PHYSICS

RESEARCH ARTICLE
Volume 17 / Issue 6 / 63502 / 2022

High T_c superconductivity in layered hydrides XH_{15} (X = Ca, Sr, Y, La) under high pressures

Yue Chen[1], Zhengtao Liu[1], Ziyue Lin[1], Qiwen Jiang[1], Mingyang Du[1], Zihan Zhang[1], Hao Song[1], Hui Xie[1], Tian Cui[2,1], Defang Duan[1,†]

1 State Key Laboratory of Superhard Materials, College of Physics, Jilin University, Changchun 130012, China
2 Institute of High Pressure Physics, School of Physical Science and Technology, Ningbo University, Ningbo 315211, China
Corresponding author. E-mail: †duandf@jlu.edu.cn
Received February 1, 2022; accepted April 25, 2022

ABSTRACT

The theoretical predictions and experimental synthesis of H_3S and LaH_{10} superconductors with record high superconducting transition temperatures (T_c) have promoted the hydrogen-based superconducors to be a research hotspot in the field of solid-state physics. Here, we predict an unprecedented layered structure CaH_{15}, with high T_c of 189 K at 200 GPa using *ab initio* calculations. As concerns the novel structure, one layer is made of a hydrogen nonagon, the other layer consists of a Ca atom and six H_2 molecular units surrounding the Ca atom. This layered structure was also found in SrH_{15}, YH_{15}, and LaH_{15} at high pressures, each materials exhibit high T_c especially YH_{15} can reach above 200 K at 220 GPa. It represents the second class of layered superhydrides with high value of T_c after pentagraphene like HfH_{10}.

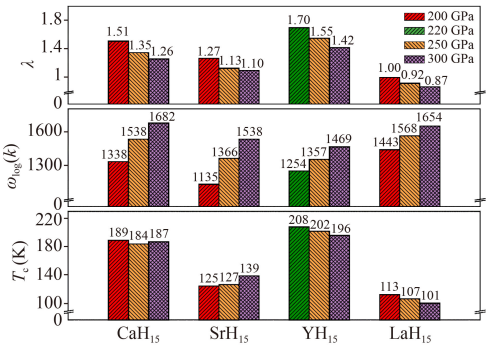

Keywords high pressure, hydrides, superconductivity, *ab initio* calculation

1 Introduction

Pressure is one of the important thermodynamic parameters that modulate the structures and properties of materials. Theory predicts that insulator molecular phase will become metallic atomic phase under enough pressures, including H_2 [1], N_2 [2], O_2 [3, 4], and F_2 [5]. Based on Bardeen–Cooper–Schrieffer (BCS) theory, metallic hydrogen with the lightest quality is predicted to be a potential room temperature superconductor [6–8]. However, utill now, there is no direct evidence in experiments to realize the metallic hydrogen at high pressures [9]. It is generally believed that at least 500 GPa may be required to achieve metallic hydrogen [10]. In order to reduce the metallization pressure of hydrogen, Ashcroft proposed the "chemical precompression" that in hydrogen-rich compounds, heavy atoms can interact with hydrogen providing chemical pressure [11]. In addition, hydrogen can provide high phonon frequencies and strong electron–phonon coupling in hydrogen-rich compounds, which make them possible to become high temperature superconductors. In the past decades, extensive researches have been conducted in field of hydrogen-based superconductors under high pressures both on theoretical prediction and experimental synthesis [12–18].

Two of the best known theories predicted hydrogen-based superconductors are H_3S [19, 20] and LaH_{10} [21, 22] which have been successfully synthesized [23–27]. H_3S has a three-dimensional S–H covalent bonds network, in which the S atoms form a bcc lattice and each S atom contacts with six H atoms, and its

https://doi.org/10.1007/s11467-022-1182-1

superconducting transition temperature (T_c) reaches 203 K at 155 GPa. LaH_{10} represents a class of three-dimensional H clathrate-like structures [21–29], in which metal atoms fill the clathrate cavities, providing electrons to stabilize the hydrogen cage and its T_c reaches 250–260 K at 170 GPa. Recently, Xie *et al.* [30] predicted a hexagonal HfH_{10} in which the H atoms arranged in clusters to form a planar "pentagraphenelike" sublattice. It is a new high temperature superconducting hydride besides covalent H_3S and cagelike LaH_{10}, with high T_c of 234 K at 250 GPa.

It is reported that there are a variety of hydrogen structural motifs in alkaline earth metal hydrides ranging from monatomic H, linear and bent H_3 molecular units to spiral polymer chains, even H_{24} and H_{29} cages [31–38]. The $C2/m$-Ca_2H_5 [31] and $I4/mmm$-CaH_4 [32] with H atoms and H_2 molecular units have been synthesized at 22 GPa and 116 GPa, respectively. The well known predicted $Im\bar{3}m$-CaH_6 with H_{24} cage [33] have been confirmed by experiments recently [34] with a maximum T_c of 215 K at 172 GPa. The $C2/m$-CaH_9 [35] with a distorted H_{29} cage was predicted to have a high T_c of 266 K at 300 GPa. The CaH_{12} with the highest H content in Ca–H system possesses three phases of $R\bar{3}$, $C2/m$ and $C2/c$ above 50 GPa [33, 35, 36], containing H_2 molecular units which are disadvantageous for high temperature superconductivity. For the Sr–H system, SrH_6 contain linear and bent H_3 molecular units transform into spiral polymer H chains at 250 GPa, and SrH_{10} posseses graphene like H-layer at high pressures [37]. Recently, experiment reported semimetallic BaH_{12} [38] contains H_2, H_3 molecular units and detached H_{12} chains with T_c of 20 K at 140 GPa. The diversity of hydrogen motifs in alkaline earth metal hydrides under high pressure led us to explore more hydrides with complex hydrogen motifs and high T_c.

Here, we performed extensive crystal structure searches on the CaH_n (n = 10–20) with high hydrogen content under high pressures. We found an interesting CaH_{15} that adopts two stacked layers, the top layer is a nonagon made of hydrogen atoms, the bottom layer consists of a Ca atom arrayed in six H_2 molecular units. The estimated T_c is about 171–189 K at 200 GPa for CaH_{15}. A new class of superhydrides, XH_{15} (X = Sr, Y, and La), which are isostructural to CaH_{15}, have also been predicted to be high temperature superconductors, especially, YH_{15} has high T_c of 192–208 K at 220 GPa.

2 Computational details

We used an *ab initio* random structure searching (AIRSS) approach [39] and the density functional theory (DFT) method as implemetend in the cambridge serial total energy package (CASTEP) [40] to predict the stable or mestable structures in CaH_n (n = 10–20), and XH_{15} (X = Sr, Y, La) between 100 and 300 GPa. In the process of structure searching, a plane-wave cut-off energy of 350 eV and a Brillouin zone sampling grid spacing of $2\pi \times 0.07$ Å^{-1} were selected.

Structural relaxations, electronic properties, and total energies were determined in the framework of DFT with Perdew–Burke–Ernzerhof parametrization of the generalized gradient approximation as implemented in the vienna *ab initio* simulation package (VASP) [41]. The valence electrons $3s^23p^64s^2$ for Ca, $4s^24p^65s^2$ for Sr, $4s^24p^64d^15s^2$ for Y, $5s^25p^65d^16s^2$ for La and $1s^1$ for H were employed with the energy cutoff of 1000 eV. The Brillouin zone was sampled with a k-point mesh of $2\pi \times 0.03$ Å^{-1} to make the enthalpy calculations well converged to less than 1 meV/atom.

Phonon dispersion and electron–phonon coupling (EPC) were carried out using density functional perturbation theory as implemented in the Quantum-ESPRESSO [42] package. Ultrasoft pseudopotentials were used with a kinetic energy cutoff of 80 Ry. The k-point and q-point meshes in the first Brillouin zone are 20×20×28 and 5×5×7 for XH_{15} (X = Ca, Sr, Y, La). The superconducting transition temperatures of these structures are estimated through the self-consistent solution of the Eliashberg equation [43, 44].

3 Results and discussion

Since hydrides with high hydrogen content are favorable for high-temperature superconductivity, we began with random structure searching for Ca–H system from 100 GPa to 300 GPa mainly focused on the stoichiometries CaH_n with n = 10–20. We compared the formation enthalpy per atom of the stable phases with CaH_2 and H_2 at selected pressures, as shown in Fig. 1. The stable structures of element H_2 [45] and binary hydrides CaH_n (n = 2, 4, 6, 9) come from the previous studies [33, 35]. The convex hull reflects the stability of each stoichiometries. The compounds located on the hull are considered to be thermodynamically stable shown in solid dots, while the compounds above the convex hull are metastable shown in hollow dots. It can be found that CaH_4 and CaH_9 are thermodynamically stable in the pressure range of 100–300 GPa, CaH_6 falls on the hull above 140 GPa, which are all in line with the previous results [33, 35]. With regard to CaH_{12}, we reproduced three phases of $R\bar{3}$, $C2/m$ and $C2/c$ under different pressures and calculated their enthalpies as a function of pressure, as shown in the Fig. S1 of supplemental materials (SM). It is found that the $R\bar{3}$ phase transforms to the $C2/m$ phase at 90 GPa, then to the $C2/c$ phase above 180 GPa. The CaH_{12} lies on the convex hull at 100–200 GPa but leaves the convex hull at 300 GPa indicating it is thermodynamically stable below 300 GPa. In addition, we found a new hydride CaH_{14} with $R\bar{3}$ symmetry

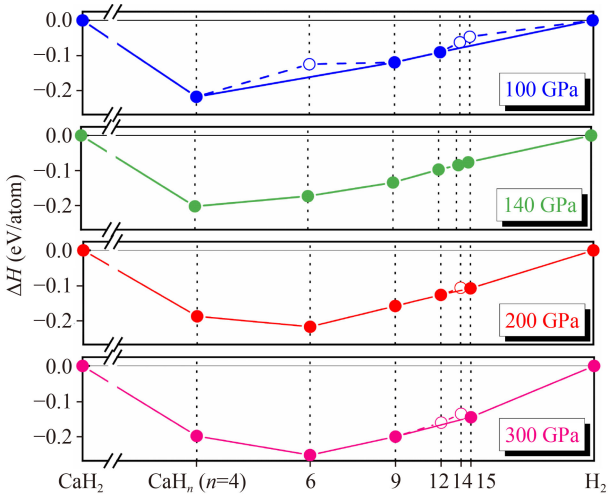

Fig. 1 The convex hull of the Ca–H system relative to CaH_2 and H_2 at 100, 140, 200, and 300 GPa.

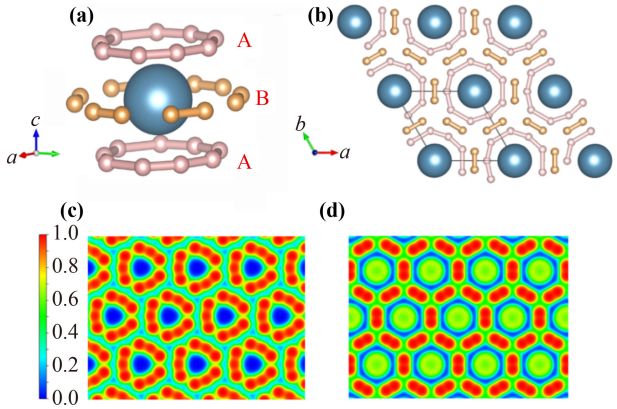

Fig. 2 **(a)** The structural model of layered $P\bar{6}2m$ in CaH_{15}, where the layers are stacked in an ABAB fashion. The A layer contains nonagon hydrogen colored pink, the B layer contains six H_2 molecules and a calcium atom colored orange and blue, respectively. **(b)** Top view of crystal structure of $P\bar{6}2m$ phase. Electron localization function of $P\bar{6}2m$-CaH_{15} at 300 GPa of **(c)** nonagon planes and **(d)** six H_2 molecules planes.

which lies on the convex hull at 140 GPa. This structure contains H_2 molecular units as shown in Fig. S2 of SM, and the lattice parameters are listed in Table S1 of SM. We will not discuss the properties of CaH_{12} and CaH_{14} in detail because they would not have good superconductivity based on the previous summarized four criteria for high T_c hydrides [30]. It is noteworthy that an unique structure $P\bar{6}2m$-CaH_{15} falls on the convex hull at pressures above 140 GPa indicating that the structure is thermodynamically stable. In addition, there is no phase transitions throughout the pressure range we studied, and the structural parameters are listed in Table S2 of SM.

We study the geometry of $P\bar{6}2m$-CaH_{15} in more detail. This layered structure are stacked in ABAB fashion in which the A layer consists of a nonagon made of hydrogen atoms, the B layer contains six H_2 molecules ring and a Ca atom located in the centre of the ring, as shown in Figs. 2(a) and (b). The calculated electronic localization function (ELF) maps and Bader charges show its chemical bonding more clear. For the A layer, nonagons [Fig. 2(c)] are actually surrounded by three curved H_3 units. The ELF values surrounding H_3 units equal 0.8 indicating that there are covalent bonding among these H atoms. High pressure strengthens the interaction between the H_3 units, and makes three H_3 units concatenate into a nine-membered ring. And it can be seen from Fig. 2(d), in B layer, the ELF value surround the neighboring H_2 molecular units is 0.5, indicating the electrons can flow in the intermolecular region of H_2. In addition, the ELF toward the neighboring H–Ca connections show none electron localization, suggesting Ca–H bonding is mainly ionic. Bader charge analysis shows that charge transfer is about 1 |e| from Ca to H proving its ionic character, as listed in Table S2 of SM.

We investigate the H–H bonding character in $P\bar{6}2m$-CaH_{15} by calculating the crystal orbital Hamiltonian population (COHP), which counts the population of wavefunctions on two atomic orbitals of a pair of selected atoms. Figures 3(a) and (b) show the top view of the hydrogen nonagon layer and H_2 molecular units layer, in which the intramolecular/intermolecular H–H distances represent by d1/d2 for hydrogen nonagon ring and d3/d4 for H_2 molecualr ring. The H–H distances are 0.877 Å (d1) and 1.051 Å (d2) for hydrogen nonagon ring, 0.832 Å (d3) and 1.14 Å (d4) for H_2 molecualr ring at 300 GPa. The COHP of $P\bar{6}2m$-CaH_{15} is shown in Fig. 3(c), the left sides with negative values represent bonding states, the right sides are antibonding states. The integrated COHP (ICOHP) up to the Fermi level represent the bonding interactions between H atoms, larger negative values represent stronger H–H bonds. The ICOHP values of those short H–H distances like 0.877, 1.051, and 0.832 Å are –3.64, –2.21, and –4.21 eV, respectively, indicating strong bonding interactions among these H atoms. These intramolecular H–H distances are longer than that of isolated H_2 molecules (0.74 Å) which is attributed to the extra electrons occupying the antibonding orbitals of hydrogen molecules, weakening the H–H bonding and increasing the bond length.

The elements Ca and Sr have similar properties: the Pauling electronegativity is 1 for Ca and 0.95 for Sr, atomic radius is 1.97 Å for Ca and 2.15 Å for Sr, and they have the same valence electron configuration. We further searched the structures of SrH_{15} between 100 and 300 GPa, and as expected we obtained the same $P\bar{6}2m$ structure as CaH_{15} which settles on the convex hull above 110 GPa, as shown in Fig. S3 of SM. In addition, the elements Y and La are diagonally adjacent with Ca and Sr in the periodic table, respectively, which may have similar structures and properties. We performed

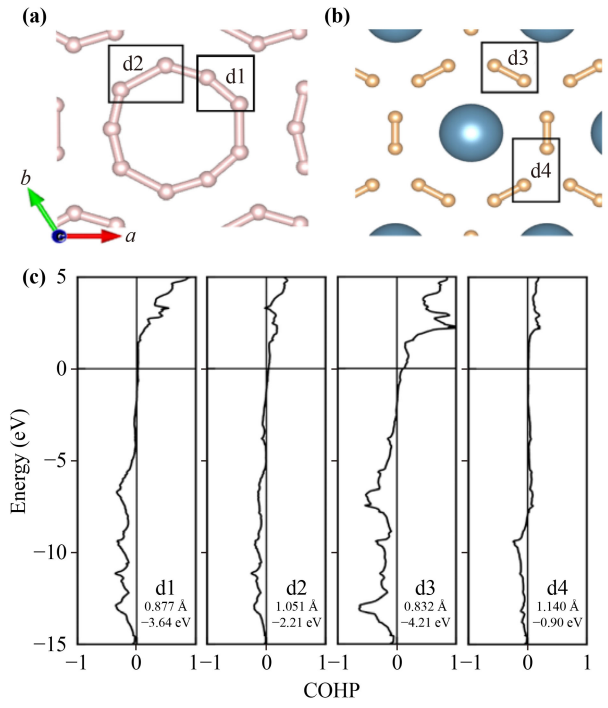

Fig. 3 Top view of **(a)** the hydrogen nonagon layer and **(b)** the H_2 molecular units layer. **(c)** The crystalline orbital Hamiltonian population (COHP) of different H–H bonds denoted as d1, d2, d3, d4 for $P\bar{6}2m$-CaH_{15} at 300 GPa.

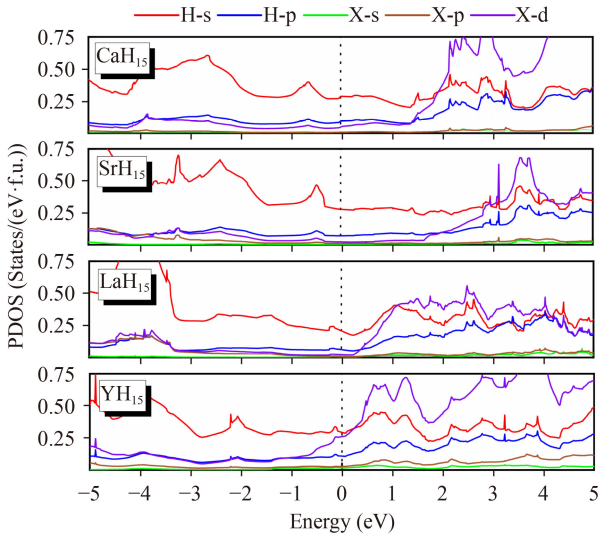

Fig. 4 Electronic density of states of CaH_{15}, SrH_{15}, YH_{15}, and LaH_{15} at 300 GPa. The red and bule lines represent the contributions of H s-orbitals and p-orbitals to the electronic density of states, and the green, brown and purple lines represent the contributions from s, p, d orbitals of metal atoms, respectively.

the random structure searching for YH_{15} and LaH_{15} at high pressures and found the same structure with CaH_{15}. Both YH_{15} and LaH_{15} are metastable which are close to the convex hull (20–33 meV/atom above tie line) at 300 GPa, as shown in Fig. S4 of SM. We note that the $P\bar{6}2m$ structure was first predicted in ErH_{15} by Dmitrii *et al.* [36], but it was not discussed in depth. The main focus of this work being on distribution of superconductivity in metal hydrides.

To further explore the electronic properties of XH_{15} (X = Ca, Sr, Y, La), we calculated the electronic band structures (Fig. S5 of SM) and partial electronic density of states (Fig. 4) of $P\bar{6}2m$-XH_{15} at 300 GPa. These four compounds have similar band structures, and they are good metal with highly dispersive bands crossing the Fermi level, especially, two bands along Γ–A–H direction are very steep (Fig. S5 of SM). From the electronic density of states in Fig. 4, we can see that the electronic states at the Fermi level are mainly contributed by H s-orbitals, which is favorable to electron phonon coupling and superconductivity. Noteworthy, the H p-orbitals also play an important role for the density of electronic states at Fermi surface. We consider that H_3 molecular units interact with each other to form a nonagon and the interaction between H_3 units is enhanced under higher pressure which requires the participation of H p-orbitals [37]. The total DOS of XH_{15} (X = Ca, Sr, Y, La) at the Fermi level are calculated to be 0.58, 0.51, 0.85 and 0.43 states/(eV·f.u.) at 300 GPa, respectively. It is worth noting that for YH_{15}, besides H s-orbitals, d-orbitals also contribute a lot to the electronic density of states at the Fermi level. So YH_{15} has the largest total DOS at the Fermi level among these four compounds.

The calculated phonon band structures, partial phonon density of states (PHDOS), eliashberg spectral functions $\alpha^2F(\omega)$, and integral EPC parameters λ of XH_{15} (X = Ca, Sr, Y, La) at 300 GPa are shown in Fig. 5. There are absent of imaginary frequency in the entire Brillouin zone for all structures, which demonstrates their dynamical stability. Due to the discrepancy of atomic mass, these PHDOS divide the contribution of λ into three parts: the low-frequency vibrational modes below 500 cm^{-1} mainly correspond to the vibrations of metal atoms X (X = Ca, Sr, Y, La) with a contribution below 30% of the total λ; the middle parts range from 500 cm^{-1} to 2200 cm^{-1} mostly come from the interaction of metal atoms and H_2 or H_3 units with a contribution about 60%–70% of the total λ; the high frequency above 2200 cm^{-1} are primarily dominated by the modes corresponding to the symmetric H_2 and H_3 stretch vibration contributed about 10%–30% to the total λ. Hydorgen atoms play a dominating role in eletron–phonon coupling, for CaH_{15} and SrH_{15}, there are distinct anomalies (dips) in the phonon dispersion curves mainly concentrated in the middle parts of vibration modes, especially the fifth and sixth vibrational modes at the A point. For YH_{15}, there is a strong dip in phonon branch 5 at the H point. For LaH_{15}, there is no distinct phonon dip (phonon softening) along the high symmetry line. In addition, we projected the EPC λ on phonon dispersion

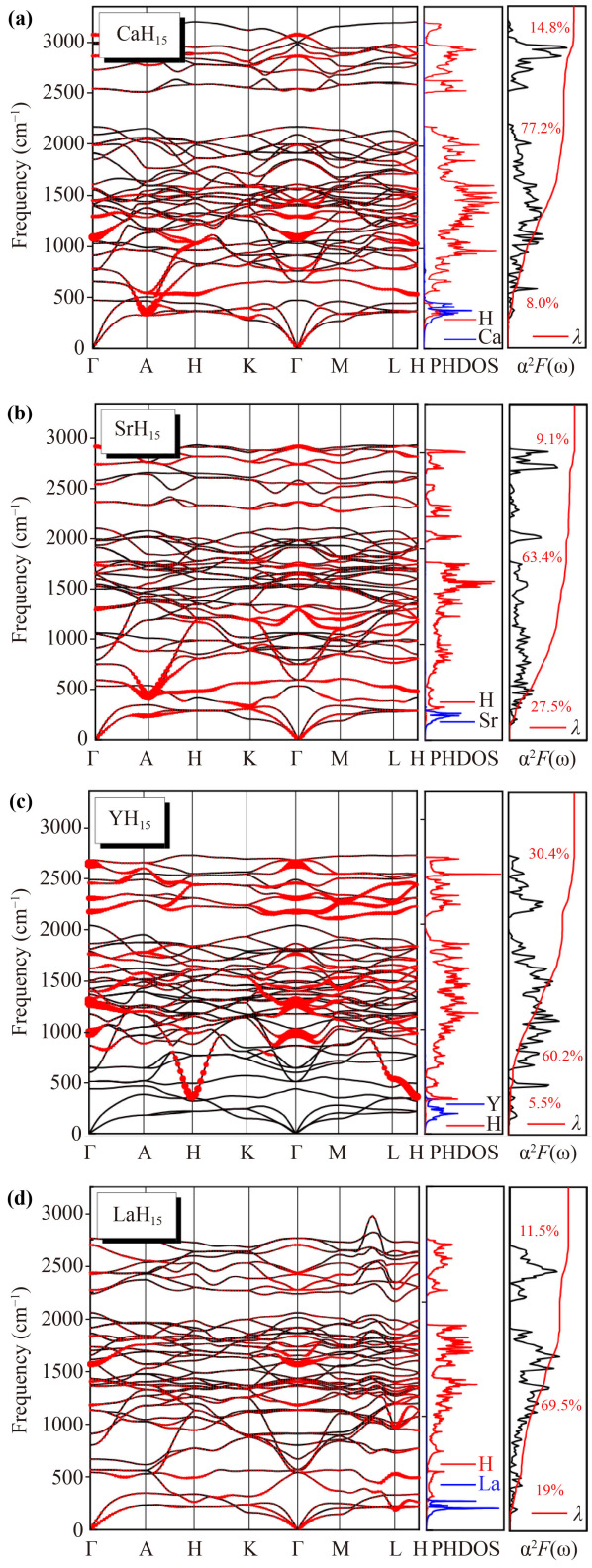

Fig. 5 The phonon band structure, PHDOS, EPC parameter λ, logarithmic average phonon frequency $\omega_{\log}$ and Eliashberg spectral function $\alpha^2F(\omega)$ of **(a)** CaH_{15}, **(b)** SrH_{15}, **(c)** YH_{15}, **(d)** LaH_{15} at 300 GPa. The size of the red solid dots on phonon dispersion curves signifies the contribution to electron–phonon coupling.

curves and the sizes of circles are proportional to the strength of λ, as shown in Fig. 5. It is clearly seen that the λ is particularly enhanced in these phonon dip regions of CaH_{15}, SrH_{15}, and YH_{15} which is favorable to produce a high superconducting transition temperature.

We show some crucial parameters involved with the superconductivity of XH_{15} (X = Ca, Sr, Y, La) compounds at different pressures including the EPC parameter λ, the logarithmic average phonon frequency $\omega_{\log}$, and the superconducting transition temperature T_c (Fig. 6). It can be seen the total λ of CaH_{15} and SrH_{15} at 300 GPa are calculated as being 1.26 and 1.10, YH_{15} has the largest λ of 1.42, while LaH_{15} has the smallest λ less than 1. The YH_{15} has the smallest $\omega_{\log}$ of 1469 K, while its λ is the highest among these four compounds, which due to the large DOS at the Fermi level and the strong phonon dips at H poinit, as shown in Fig. 4 and Fig. 5. As the case of LaH_{15}, it renders to produce a relative high $\omega_{\log}$ but small λ, due to the hard phonon modes and the small DOS at the Fermi level. The Coulomb pseudopotential μ^* is often taking from 0.1 to 0.13 for hydrogen-dominant metallic alloys. Using μ^* values of 0.1 and 0.13, the ranges of T_c values for the compouds CaH_{15}, SrH_{15}, YH_{15}, LaH_{15} are estimated to be 168–187 K, 122–139 K, 177–196 K and 85–101 K at 300 GPa, respectively, via the numerical solution of Eliashberg equation. It can be seen that T_c decreases in the order of YH_{15} > CaH_{15} > SrH_{15} >LaH_{15}, consistent with the decreasing trend of λ. Thus, the high T_c in these hydrides is mainly attributed to the EPC interaction. With decreasing pressures, the electron–phonon coupling parameter λ of XH_{15} (X = Ca, Sr, Y, La) raise, while logarithmic average phonon frequency $\omega_{\log}$ decrease. But superconducting transition temperature T_cs of these four compounds are somewhat different. In case of CaH_{15}, the λ increases to 1.51, the $\omega_{\log}$ decreases to 1338 K, and the T_c reaches maximum of 189 K with μ^* = 0.1 (177 K with μ^* = 0.13) at 200 GPa which is only 2 K higher

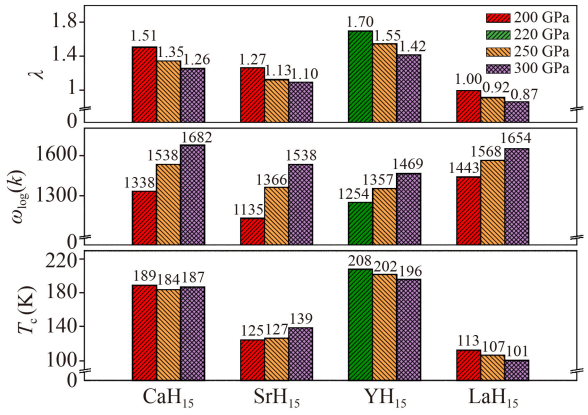

Fig. 6 The calculated electron–phonon coupling parameter λ (top panel), logarithmic average phonon frequency $\omega_{\log}$ (middle panel), and T_c with μ^* = 0.1 (bottom panel) of XH_{15} (X = Ca, Sr, Y, La) at different pressures.

than T_c at 300 GPa. The estimated T_c of YH_{15} increases with decreasing pressure at the rate of –0.15 K/GPa (dT_c/dP) and reaches maximum of 208 K with $\mu^* = 0.1$ (192 K with $\mu^* = 0.13$) at 220 GPa, exceeding the T_c (203 K) of H_3S. The pressure dependence T_c of LaH_{15} is –0.12 K/GPa which is similar with that of YH_{15}, and the maximum T_c reaches 113 K with $\mu^* = 0.1$ at 200 GPa (100 K with $\mu^* = 0.13$). On the contrary, the T_c of SrH_{15} decreases with decreasing pressure and reduces to 125 K with $\mu^* = 0.1$ at 200 GPa (111 K with $\mu^* = 0.13$). Although the T_cs of XH_{15} (X = Ca, Sr, Y, La) dependence on pressure are different, they do not change much. This effect is the consequence of a complicated balance between the λ and ω_{log} at different pressures.

4 Conclusions

We have used *ab initio* random structure searching approach to explore the crystal structures of CaH_n (n = 10–20) from 100 to 300 GPa and found a unique layer structure with hydrogen nonagon, $P\bar{6}2m$-CaH_{15}, which was calculated to be thermodynamical stable above 140 GPa. The same hydrogen nonagon structure was also found in SrH_{15}, YH_{15} and LaH_{15} under high pressures. The SrH_{15} is thermodynamical stable above 110 GPa, while YH_{15} and LaH_{15} are metastable in our studied pressure range. Electron–phonon coupling calculations show that the XH_{15} (X = Ca, Sr, Y, La) are potentially high temperature superconductors with estimated maximum T_c of 189 K at 200 GPa, 139 K at 300 GPa, 208 K at 220 GPa and 113 K at 200 GPa, respectively. The YH_{15} has the highest T_c among these four compounds due to the largest λ which is attributed to the strong phonon dips at H point and large DOS at the Fermi level. Further calculations show that the superconducting critical temperature of XH_{15} (X = Ca, Sr, Y, La) has only a weak dependence on pressure due to the banlance of the λ and ω_{log} at different pressures. Our work will stimulate the future discovery of more layered class of high temperature superconductors in compressed hydrides.

Note: This paper is dedicated to the 70th anniversary of the physics of Jilin University.

Electronic supplementary materials are available in the online version of this article at https://doi.org/10.1007/s11467-022-1182-1 and https://journal.hep.com.cn/fop/EN/10.1007/s11467-022-1182-1 and are accessible for authorized users. See Supplemental Material for the structural information, Bader charge analysis and band structures of CaH_{15}, enthalpy difference curves of CaH_{12}, structural information and crystal structure of CaH_{14}, as well as convex hull diagram of Sr–H, Y–H and La–H system under high pressures.

Acknowledgements This work was supported by the National Natural Science Foundation of China (Grant Nos. 12122405, 52072188, and 51632002), the National Key R&D Program of China (Grant No. 2018YFA0305900), and the Jilin Provincial Science and Technology Development Project (20210509038RQ). Parts of the calculations were performed in the High Performance Computing Center (HPCC) of Jilin University and TianHe-1(A) at the National Supercomputer Center in Tianjin.

References

1. J. M. McMahon and D. M. Ceperley, Ground-state structures of atomic metallic hydrogen, *Phys. Rev. Lett.* 106(16), 165302 (2011)
2. J. Sun, M. Martinez-Canales, D. D. Klug, C. J. Pickard, and R. J. Needs, Stable all-nitrogen metallic salt at terapascal pressures, *Phys. Rev. Lett.* 111(17), 175502 (2013)
3. J. Sun, M. Martinez-Canales, D. D. Klug, C. J. Pickard, and R. J. Needs, Persistence and eventual demise of oxygen molecules at terapascal pressures, *Phys. Rev. Lett.* 108(4), 045503 (2012)
4. L. Zhu, Z. Wang, Y. Wang, G. Zou, H. K. Mao, and Y. Ma, Spiral chain O_4 form of dense oxygen, *Proc. Natl. Acad. Sci. USA* 109(3), 751 (2012)
5. D. Duan, Z. Liu, Z. Lin, H. Song, H. Xie, T. Cui, C. J. Pickard, and M. Miao, Multistep dissociation of fluorine molecules under extreme compression, *Phys. Rev. Lett.* 126(22), 225704 (2021)
6. E. Wigner and H. B. Huntington, On the possibility of a metallic modification of hydrogen, *J. Chem. Phys.* 3(12), 764 (1935)
7. N. W. Ashcroft, Metallic hydrogen: A high-temperature superconductor, *Phys. Rev. Lett.* 21(26), 1748 (1968)
8. J. M. McMahon and D. M. Ceperley, High-temperature superconductivity in atomic metallic hydrogen, *Phys. Rev. B* 84(14), 144515 (2011)
9. R. P. Dias and I. F. Silvera, Observation of the Wigner–Huntington transition to metallic hydrogen, *Science* 355(6326), 715 (2017)
10. J. M. McMahon and D. M. Ceperley, Ground-state structures of atomic metallic hydrogen, *Phys. Rev. Lett.* 106(16), 165302 (2011)
11. N. W. Ashcroft, Hydrogen dominant metallic alloys: High temperature superconductors, *Phys. Rev. Lett.* 92(18), 187002 (2004)
12. L. Zhang, Y. Wang, J. Lv, and Y. Ma, Materials discovery at high pressures, *Nat. Rev. Mater.* 2(4), 17005 (2017)
13. M. Du, W. Zhao, T. Cui, and D. Duan, Compressed superhydrides: The road to room temperature superconductivity, *J. Phys.: Condens. Matter* 34(17), 173001 (2022)
14. D. Duan, Y. Liu, Y. Ma, Z. Shao, B. Liu, and T. Cui, Structure and superconductivity of hydrides at high pressures, *Natl. Sci. Rev.* 4(1), 121 (2017)
15. X. H. Xiao, D. F. Duan, Y. B. Ma, H. Xie, H. Song, D. Li, F. B. Tian, B. B. Liu, H. Y. Yu, and T. Cui, *Ab initio* studies of copper hydrides under high pressure, *Front. Phys.* 14(4), 1 (2019)
16. L. P. Gor'kov and V. Z. Kresin, Colloquium: High pressure and road to room temperature superconductivity, *Rev. Mod. Phys.* 90(1), 011001 (2018)
17. E. Zurek, Hydrides of the alkali metals and alkaline earth metals under pressure, *Comments Inorg. Chem.*

37(2), 78 (2017)
18. Z. Zhang, T. Cui, M. J. Hutcheon, A. M. Shipley, H. Song, M. Du, V. Z. Kresin, D. Duan, C. J. Pickard, and Y. Yao, Design principles for high-temperature superconductors with a hydrogen-based alloy backbone at moderate pressure, *Phys. Rev. Lett.* 128(4), 047001 (2022)
19. D. Duan, Y. Liu, F. Tian, D. Li, X. Huang, Z. Zhao, H. Yu, B. Liu, W. Tian, and T. Cui, Pressure-induced metallization of dense $(H_2S)_2H_2$ with high-T_c superconductivity, *Sci. Rep.* 4(1), 6968 (2015)
20. D. Duan, X. Huang, F. Tian, D. Li, H. Yu, Y. Liu, Y. Ma, B. Liu, and T. Cui, Pressure-induced decomposition of solid hydrogen sulfide, *Phys. Rev. B* 91(18), 180502 (2015)
21. H. Liu, I. I. Naumov, R. Hoffmann, N. W. Ashcroft, and R. J. Hemley, Potential high-T_c superconducting lanthanum and yttrium hydrides at high pressure, *Proc. Natl. Acad. Sci. USA* 114(27), 6990 (2017)
22. F. Peng, Y. Sun, C. J. Pickard, R. J. Needs, Q. Wu, and Y. Ma, Hydrogen clathrate structures in rare earth hydrides at high pressures: Possible route to room-temperature superconductivity, *Phys. Rev. Lett.* 119(10), 107001 (2017)
23. A. P. Drozdov, M. I. Eremets, I. A. Troyan, V. Ksenofontov, and S. I. Shylin, Conventional superconductivity at 203 kelvin at high pressures in the sulfur hydride system, *Nature* 525(7567), 73 (2015)
24. M. Einaga, M. Sakata, T. Ishikawa, K. Shimizu, M. I. Eremets, A. P. Drozdov, I. A. Troyan, N. Hirao, and Y. Ohishi, Crystal structure of the superconducting phase of sulfur hydride, *Nat. Phys.* 12(9), 835 (2016)
25. A. P. Drozdov, P. P. Kong, V. S. Minkov, S. P. Besedin, M. A. Kuzovnikov, S. Mozaffari, L. Balicas, F. F. Balakirev, D. E. Graf, V. B. Prakapenka, E. Greenberg, D. A. Knyazev, M. Tkacz, and M. I. Eremets, Superconductivity at 250 K in lanthanum hydride under high pressures, *Nature* 569(7757), 528 (2019)
26. M. Somayazulu, M. Ahart, A. K. Mishra, Z. M. Geballe, M. Baldini, Y. Meng, V. V. Struzhkin, and R. J. Hemley, Evidence for superconductivity above 260 K in lanthanum superhydride at megabar pressures, *Phys. Rev. Lett.* 122(2), 027001 (2019)
27. Y. Li, J. Hao, H. Liu, J. Tse, Y. Wang, and Y. Ma, Pressure-stabilized superconductive yttrium hydrides, *Sci. Rep.* 5(1), 9948 (2015)
28. H. Song, Z. Zhang, T. Cui, C. J. Pickard, V. Z. Kresin, and D. Duan, High T_c superconductivity in heavy rare earth hydrides, *Chin. Phys. Lett.* 38(10), 107401 (2021)
29. X. Zhong, Y. Sun, T. Iitaka, M. Xu, H. Liu, C. Chen and Y. Ma, Potential room temperature superconductivity in clathrate lanthanide/actinides octadechydrides at extreme pressures, doi: 10.21203/rs.3.rs-1148583/v1 (2021)
30. H. Xie, Y. Yao, X. Feng, D. Duan, H. Song, Z. Zhang, S. Jiang, S. A. T. Redfern, V. Z. Kresin, C. J. Pickard, and T. Cui, Hydrogen pentagraphenelike structure stabilized by hafnium: A high-temperature conventional superconductor, *Phys. Rev. Lett.* 125(21), 217001 (2020)
31. A. K. Mishra, T. Muramatsu, H. Liu, Z. M. Geballe, M. Somayazulu, M. Ahart, M. Baldini, Y. Meng, E. Zurek, and R. J. Hemley, New calcium hydrides with mixed atomic and molecular hydrogen, *J. Phys. Chem. C* 122(34), 19370 (2018)
32. G. Wu, X. Huang, H. Xie, X. Li, M. Liu, Y. Liang, Y. Huang, D. Duan, F. Li, B. Liu, and T. Cui, Unexpected calcium polyhydride CaH_4: A possible route to dissociation of hydrogen molecules, *J. Chem. Phys.* 150(4), 044507 (2019)
33. H. Wang, J. S. Tse, K. Tanaka, T. Iitaka, and Y. Ma, Superconductive sodalite-like clathrate calcium hydride at high pressures, *Proc. Natl. Acad. Sci. USA* 109(17), 6463 (2012)
34. L. Ma, K. Wang, Y. Xie, X. Yang, Y. Wang, M. Zhou, H. Liu, G. Liu, H. Wang, and Y. Ma, High-T_c superconductivity in clathrate calcium hydride CaH_6, arXiv: 2103.16282 (2021)
35. Z. Shao, D. Duan, Y. Ma, H. Yu, H. Song, H. Xie, D. Li, F. Tian, B. Liu, and T. Cui, Unique phase diagram and superconductivity of calcium hydrides at high pressures, *Inorg. Chem.* 58(4), 2558 (2019)
36. D. V. Semenok, D. Zhou, A. G. Kvashnin, X. Huang, M. Galasso, I. A. Kruglov, A. G. Ivanova, A. G. Gavriliuk, W. Chen, N. V. Tkachenko, A. I. Boldyrev, I. Troyan, A. R. Oganov, and T. Cui, Novel strongly correlated europium superhydrides, *J. Phys. Chem. Lett.* 12(1), 32 (2021)
37. Y. Wang, H. Wang, J. S. Tse, T. Iitaka, and Y. Ma, Structural morphologies of high-pressure polymorphs of strontium hydrides, *Phys. Chem. Chem. Phys.* 17(29), 19379 (2015)
38. W. Chen, D. V. Semenok, A. G. Kvashnin, X. Huang, I. A. Kruglov, M. Galasso, H. Song, D. Duan, A. F. Goncharov, V. B. Prakapenka, A. R. Oganov, and T. Cui, Synthesis of molecular metallic barium superhydride: Pseudocubic BaH_{12}, *Nat. Commun.* 12(1), 273 (2021)
39. C. J. Pickard and R. J. Needs, *Ab initio* random structure searching, *J. Phys.: Condens. Matter* 23(5), 053201 (2011)
40. S. J. Clark, M. D. Segall, C. J. Pickard, P. J. Hasnip, M. J. Probert, K. Refson, and M. C. Payne, First principles methods using CASTEP, *Z. Kristallogr. Cryst. Mater.* 220(5–6), 567 (2005)
41. G. Kresse and J. Furthmuller, Efficient iterative schemes for *ab initio* total-energy calculations using a plane-wave basis set, *Phys. Rev. B* 54(16), 11169 (1996)
42. P. Giannozzi, S. Baroni, N. Bonini, M. Calandra, R. Car, C. Cavazzoni, D. Ceresoli, G. L. Chiarotti, M. Cococcioni, I. Dabo, A. Dal Corso, S. de Gironcoli, S. Fabris, G. Fratesi, R. Gebauer, U. Gerstmann, C. Gougoussis, A. Kokalj, M. Lazzeri, L. Martin-Samos, N. Marzari, F. Mauri, R. Mazzarello, S. Paolini, A. Pasquarello, L. Paulatto, C. Sbraccia, S. Scandolo, G. Sclauzero, A. P. Seitsonen, A. Smogunov, P. Umari, and R. M. Wentzcovitch, QUANTUM ESPRESSO: A modular and open-source software project for quantum simulations of materials, *J. Phys.: Condens. Matter* 21(39), 395502 (2009)
43. W. L. McMillan, Transition temperature of strong-coupled superconductors, *Phys. Rev.* 167(2), 331 (1968)
44. G. M. Eliashberg, Interactions between electrons and lattice vibrations in a superconductor, *Sov. Phys. JETP* 11(3), 696 (1960)
45. C. J. Pickard and R. J. Needs, Structure of phase III of solid hydrogen, *Nat. Phys.* 3(7), 473 (2007)